RSC Advances

PAPER

View Article Online
View Journal | View Issue

Cite this: *RSC Adv.*, 2017, **7**, 48176

Piezotronic-effect-enhanced Ag_2S/ZnO photocatalyst for organic dye degradation†

Yang Zhang, ‡[a] Caihong Liu,‡[a] Gaolong Zhu,[b] Xin Huang,[a] Wei Liu,[a] Weiguo Hu,[a] Ming Song,[a] Weidong He,[b] Juan Liu*[c] and Junyi Zhai *[a]

Received 14th September 2017
Accepted 2nd October 2017

DOI: 10.1039/c7ra10206b

rsc.li/rsc-advances

Taking advantage of the piezotronic effect, enhanced photocatalytic performance of a Ag_2S@ZnO hybrid photocatalyst was achieved under sonication. Decorating Ag_2S (~1.4 eV bandgap) nanoparticles on ZnO (~3.3 eV bandgap) nanowire surfaces successfully extended the light response to the visible light range. The formation of type II band alignment at the Ag_2S/ZnO heterointerface facilitated the separation of photoexcited electrons and holes, promoting utilization of photoexcited charge carriers in the photocatalytic process. Furthermore, the strain-generated positive piezocharges effectively lowered the barrier height, considerably motivating charge transport across the Ag_2S/ZnO heterointerface, which further boosted the hybrid photocatalyst performance. The high reproducibility of the photocatalytic activities indicated that the modification of ZnO nanowires with Ag_2S nanoparticles effectively stabilized the photocatalyst in reactions. The degradation rate of Ag_2S@ZnO nanowires remained at $C/C_0 = 18.6\%$ after eight cycles, while bare ZnO nanowires exhibited poorer performance ($C/C_0 = 48.1\%$). This study showed the effectiveness of using the piezotronic effect in water purification and recovery by combined use of solar and mechanical energy.

Introduction

Recycling and reusing wastewater is a recognized strategic approach to addressing the increasing demand for, and shortage of, clean water sources.[1–4] Consequently, considerable effort has been devoted to developing techniques to eliminate toxic chemicals, such as organic dyes, from wastewater. Solar photocatalytic methods have been extensively studied as low-cost, environmentally friendly, and sustainable technologies for wastewater treatment.[5–7] In photocatalytic reactions, semiconductors can utilize clean and renewable solar energy to catalyze reactions on photocatalyst surfaces *via* photoexcited holes and electrons when the incident photon energy is greater than the band gap of the semiconductor material.[8,9] Previous studies have demonstrated that nanostructured semiconductor-based photocatalysts can be widely employed to eliminate various organic pollutants in an environmentally sustainable manner.[10–13] However, the rapid recombination of photoexcited electron–hole pairs is the principal obstacle to the development of highly efficient photocatalysts.[14] Therefore, tremendous effort has been focused on reducing the recombination probability of photoexcited electron–hole pairs by constructing hybrid photocatalytic systems.[8,15,16]

Different kinds of hybrid photocatalysts can inhibit the fast recombination of photoexcited electron–hole pairs through different mechanisms. For semiconductor/metal composite photocatalysts, photoexcited electrons can be transferred relatively easily from semiconductors to metal nanoparticles *via* Schottky contact due to the Fermi energy of the selected metals usually being lower than that of the semiconductors.[17] However, the metals utilized in this kind of hybrid photocatalyst have largely been limited to noble metals, such as Ag, Au, Pt, and Pd.[18–21] Transition metals, such as Cu, Co, and Ni, have been investigated in an attempt to replace noble metals.[22–24] In semiconductor/semiconductor hybrid photocatalysts, metal oxides and sulfides have been extensively applied to construct heterojunctions/interfaces that can effectively facilitate the spatial separation of photoexcited electron–hole pairs using suitable band alignment. In particular, for type II heterojunctions/interfaces, photoexcited electrons tend to transfer from the semiconductor with a narrower band gap to that with a wider band gap, while photoexcited holes often transfer in the opposite direction due to the relative positions of the valence band (VB) and conduction band (CB). Furthermore, using semiconductors with a narrow band gap in the composites can extend the light response range of the photocatalysts

[a]*Beijing Institute of Nanoenergy and Nanosystems, Chinese Academy of Sciences, National Center for Nanoscience and Technology (NCNST), Beijing, 100083, China. E-mail: jyzhai@binn.cas.cn*

[b]*School of Energy Science and Engineering, University of Electronic Science and Technology, Chengdu, Sichuan, 611731, China*

[c]*College of Environmental Sciences and Engineering, Peking University, Beijing, 100871, China. E-mail: juan.liu@pku.edu.cn*

† Electronic supplementary information (ESI) available. See DOI: 10.1039/c7ra10206b

‡ These authors contributed equally.

into the visible light region, which is an important characteristic for promoting the efficiency of the hybrid photocatalysts in practical applications.[25]

Among all metal oxide/sulfide semiconductors, wurtzite-structured ZnO has received much attention as a multifunctional and high-performance material for optoelectronic devices, photodetectors, dye-sensitized solar cells, energy harvesting devices, and photocatalysts.[26–35] Many previous studies have been conducted to enhance the photocatalytic activity of ZnO using different morphologies, including nanoparticles, nanotubes, and hollow spheres.[36–39] The basic strategies for improving the photocatalytic activity of ZnO are extending the light response range and inhibiting the photoexcited charge carrier recombination. Although metal sulfides (M_xS) have been extensively used as photocatalysts, until recently they have not been employed in photocatalytic composites.[40,41] M_xS/ZnO composites show great potential for enhanced photocatalytic performance under mechanical strain conditions because the piezopotential intentionally introduced in the M_xS/ZnO composite can theoretically facilitate the separation of photoexcited electron–hole pairs.

In this work, we report a convenient and effective approach to prepare Ag_2S@ZnO nanowires (NWs), and investigate their photocatalytic activity in the degradation of methylene blue (MB) assisted by sonication and under light irradiation. The photocatalytic activity of Ag_2S@ZnO NWs was boosted by enhancing the separation of photoexcited electrons and holes using strain-generated piezopotentials/piezocharges. Moreover, the high reproducibility of the photocatalytic activities implied that decorating ZnO NWs with Ag_2S nanoparticles (NPs) effectively stabilized the photocatalyst in reactions. Recycling experiments showed that the Ag_2S@ZnO composite was an effective and reusable photocatalyst for organic dyes degradation. This study opens up new possibilities for designing highly efficient hybrid photocatalysts with both piezoelectric and photocatalytic characteristics that show enhanced performance in the degradation of organic contaminants. Furthermore, the proposed strategy provides valuable knowledge not only for ZnO, but also for other piezoelectric materials with smaller band gaps.

Experimental section

Synthesis of materials

ZnO NWs were synthesized using a modified hydrothermal method. In the first step, a 100 nm-thick ZnO seed layer was sequentially grown on the surface of a carbon fiber using RF magnetron sputtering at room temperature. In the second step, zinc nitrate hexahydrate (25 mM) and ammonium hydroxide (25 wt%, 10 mL) were combined to prepare a nutrient solution. After immersing the ZnO-coated CFs in the nutrient solution, the bottle was sealed, heated to 95 °C in an oven, and held at that temperature for 12 h. In the second step, the obtained ZnO NWs were thoroughly rinsed with deionized water and dried in air at 40 °C for 12 h. In the final step, Ag_2S NPs were deposited on the surface of the ZnO NWs using a successive ionic layer adsorption and reaction (SILAR) method. In this step, 10 mM Na_2S aqueous solution and 10 mM $AgNO_3$ aqueous solution were used as precursor solutions for S^{2-} and Ag^+, respectively. Ten cycles of the SILAR reaction afforded Ag_2S@ZnO NWs. Ag_2S@ZnO NWs were washed with the amount of deionized water necessary to remove residual chemicals and then dried in a vacuum oven at 40 °C for 12 h. The weight ratio of Ag_2S@ZnO composite to CFs was determined as about 1 : 1.5 by weighing samples before and after loading with Ag_2S@ZnO composites.

Materials characterization

Morphology and structural characterizations were investigated by a field-emission scanning electron microscopy (FE-SEM; SU8020), high resolution transmission electron microscopy (HRTEM; F20) and X-ray diffraction (XRD; Panalytical X'Pert Pro MPD with Cu Kα (λ = 0.15406 nm) radiation). An individual Ag_2S@ZnO NW was mechanically peeled from the carbon fiber for HRTEM characterization. UV-visible (UV-Vis) absorption spectra were recorded using a Shimadzu UV-3600 spectrometer. X-ray photoelectron spectroscopy (XPS) characterization was conducted using a Thermo Scientific ESCALAB 250Xi instrument.

Finite element method (FEM) calculations

To schematically illustrate the piezopotential, an applied strain of 50 MPa was chosen. Based on our SEM characterization, the average length and diameter of the ZnO NWs were estimated to be 8 μm and 300 nm, respectively. Elastic constants, piezoelectric constants, and relative dielectric constants were employed as described in a previous publication.[34]

Photocatalytic degradation of MB

The catalytic performance was evaluated by the degradation of an aqueous solution of MB ($C_0 = 1$ mg L^{-1}) at 20 °C under light irradiation and sonication conditions. In a typical experiment, the as-prepared photocatalysts were immersed in MB aqueous solution (100 mL) and the solution was gently stirred under ambient conditions for 30 min in the dark to reach an adsorption/desorption equilibrium. The solution was then exposed to light irradiation from simulated solar light (PerfectLight FX300, 320–800 nm) and sonication (KQ-100VDE). The light irradiation intensity and sonication frequency were determined to be 80 mW cm^{-2} and 45 KHz, respectively. At certain time intervals, aliquots (0.3 mL) of the MB aqueous solution were extracted for UV-Vis characterization. The degradation rate was characterized by measuring the absorption spectra of the MB aqueous solution and calculating the signal intensity at 665 nm.

Results and discussion

The Ag_2S@ZnO NWs hybrid photocatalyst was fabricated using the process shown in Fig. 1. Firstly, 100 nm-thick ZnO seed-layer-coated carbon fibers (CFs) 1 × 1 mm^2 in size were prepared using a radio-frequency (RF) magnetron sputtering technique, as shown in Fig. 1a. Secondly, ZnO NWs were grown on CFs using a modified hydrothermal method. Notably, the

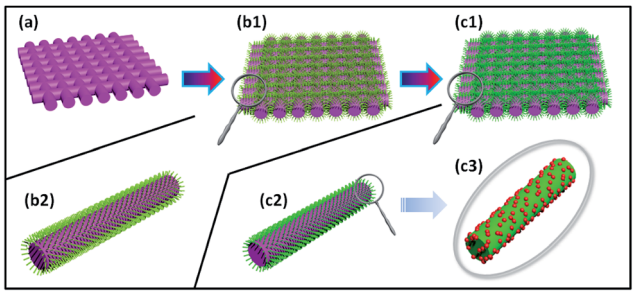

Fig. 1 Schematic diagram illustrating the synthesis of Ag_2S@ZnO NWs. (a) Bare CFs, (b1, b2) ZnO NWs synthesized by a modified hydrothermal method, and (c1–c3) Ag_2S@ZnO NWs prepared using the SILAR method. Pink, green, and red colored sections represent CFs, ZnO NWs, and Ag_2S NPs, respectively.

ZnO NWs were vertically aligned on the CF backbones (Fig. 1b). Finally, Ag_2S NPs were deposited on the ZnO NW surfaces using a SILAR method (Fig. 1c). Detailed descriptions of the syntheses of ZnO and Ag_2S@ZnO NWs are provided in the Experimental section. The as-prepared ZnO or Ag_2S@ZnO NW samples were immersed in MB aqueous solution to decompose the MB organic dye using light irradiation and continuous sonication.

The morphology and structure of ZnO NW and Ag_2S@ZnO NW photocatalysts were characterized using SEM, XPS, energy-dispersive X-ray spectroscopy (EDX), XRD, and HRTEM. Fig. 2a shows a SEM image of as-synthesized ZnO NWs. The ZnO NWs with a smooth surface were vertically aligned uniformly on the backbones of CFs. After Ag_2S deposition using the SILAR method, Ag_2S NPs were found to be well distributed on the ZnO NW surfaces, leading to a rough surface, with some aggregation of the NPs at the top of ZnO NWs (Fig. 2b).[42] Fig. 2c and d show the XPS and EDX spectra of Ag_2S@ZnO NWs on CFs, which exhibited unambiguous signals from Zn, O, Ag, and S in the as-synthesized sample. The carbon signal originated from the CFs and the Al signal from sample holder. To investigate the chemical states of Ag_2S@ZnO, the C 1s signal (284.8 eV) was used for calibration. In addition to Zn $2p_{3/2}$, Zn $2p_{1/2}$, and O 1s signals of ZnO NWs, characteristic peaks for Ag $3d_{5/2}$, Ag $3d_{3/2}$, S $2p_{3/2}$, and S $2p_{1/2}$ were observed and assigned to the deposition of Ag_2S NPs, in good agreement with previous studies. XPS results showed that only characteristic Ag $3d_{5/2}$ (368.3 eV) and Ag $3d_{3/2}$ (374.4 eV) peaks of Ag^+ were detected in the sample, with no Ag^0 peak found.[43] The atomic percentages given by the EDX spectrum for Ag and S elements present in Ag_2S@ZnO were 35.9% and 18.0%, which were close to 2 : 1. ZnO and Ag_2S@ZnO NWs were also characterized by XRD (Fig. 1e). Sharp peaks denoted with ★ and ■ were indexed to wurtzite-structured ZnO and monoclinic-structured Ag_2S, respectively.[44–46] HRTEM characterization of the Ag_2S@ZnO NWs provided convincing evidence of a heterointerface formed by Ag_2S NPs and ZnO NW. As shown in Fig. 2f, two sets of lattice fringes were identified and correlated to ZnO and Ag_2S. The spacing of 0.52 nm between lattice planes corresponded to the distance of the ZnO (0002) plane, which indicated the growth direction of individual ZnO NWs, while the adjacent spacing of 0.22 nm corresponded to the Ag_2S (031) plane.[47]

The photocatalytic performance of semiconductors or semiconductor composites essentially depends on their light absorption behavior. Therefore, light harvesting ability is a crucial parameter for investigating the photocatalytic efficiency of ZnO and Ag_2S@ZnO NWs. According to previous work, UV-Vis absorption spectroscopy analysis provided information on the light absorption ability of the catalyst.[48–50] However, in this work, the decorated catalysts being attached to CFs has a significant impact on the UV-Vis absorption process.

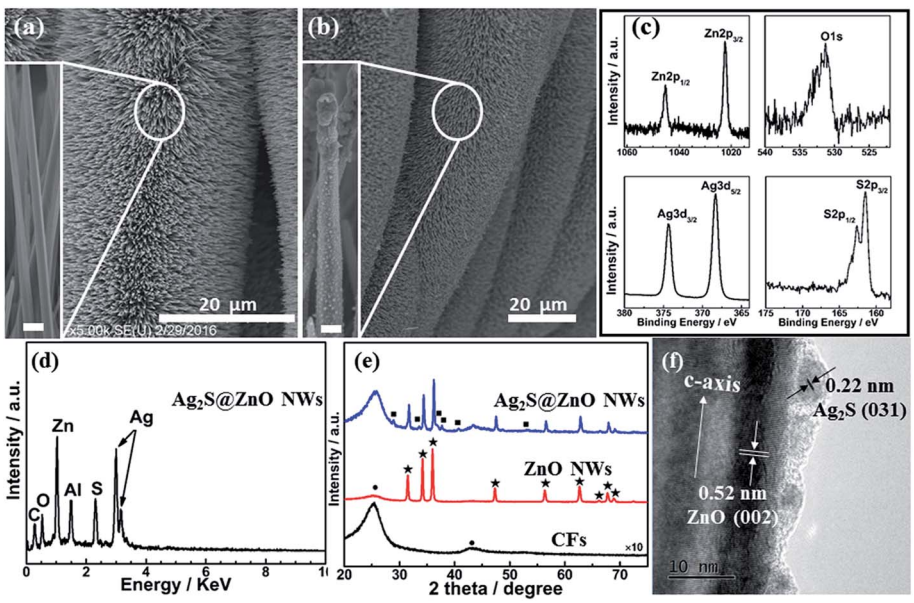

Fig. 2 SEM images of (a) ZnO NWs and (b) Ag_2S@ZnO NWs on CFs; (c) XPS spectra of Ag_2S@ZnO NWs; (d) EDX spectrum of Ag_2S@ZnO NWs; (e) XRD spectra of bare CFs, ZnO, and Ag_2S@ZnO NWs on CFs; (f) HRTEM image of a single Ag_2S@ZnO NW.

Therefore, we first synthesized ZnO NWs on transparent indium–tin oxide (ITO) substrate using the same hydrothermal conditions and performed subsequent deposition of Ag_2S NPs using the SILAR method for UV-Vis absorption spectroscopy analysis. As shown in Fig. S1 (ESI†), the absorption edge shifted from 380 nm for ZnO to 600 nm for Ag_2S@ZnO, and the absorption intensity increased after loading with Ag_2S NPs. The broader and stronger absorption characteristics of Ag_2S@ZnO NWs compared with bare ZnO NWs were explained by the formation of heterojunctions/interfaces that modified the optical absorption properties. Due to their more efficient utilization of visible light as a large part of the solar spectrum, heterostructured and multicomponent materials are interesting as potential highly efficient photocatalysts for decomposing organic pollutions. Nevertheless, the piezoelectric characteristics of 1D ZnO-based piezoelectric composite have rarely been considered and exploited in photocatalytic reactions.[34,51]

The working mechanism of the piezopotential/piezocharge-enhanced photocatalytic performance of ZnO and Ag_2S@ZnO NWs is discussed below. MB was employed as a representative organic pollutant to investigate the photocatalytic performance of as-prepared samples under light illumination and sonication conditions. By illuminating the as-prepared ZnO NWs with UV light, the electrons in the VB are excited to the CB, while an equal number of holes are left in the VB, as shown in Fig. 3a. For ZnO NWs without Ag_2S NPs, the photoexcited holes can react with hydroxyl groups to produce free hydroxyl radicals ($^{\cdot}OH$). The photoexcited electrons can react with O_2 to produce $^{\cdot}O_2^-$, $^{\cdot}HO_2$, H_2O_2, and $^{\cdot}OH$ radicals. These radicals then decompose MB to CO_2, H_2O, and nontoxic substances in aqueous solution.

Under sonic wave excitation in liquid with the generation of bubbles, the complex turbulence in the solution around the fibers can cause the ZnO NWs to bend, which generates a piezoelectric potential across the width of the nanowires. The piezopotential distribution in ZnO NWs was calculated using FEM. Details of these FEM calculations are provided in the Experimental section. As shown in the cross-section view of a single ZnO NW in Fig. S2 (ESI†), the strain-generated piezopotential was parallel to the growth direction of the ZnO NW. Under light illumination and sonication conditions, this strain-generated piezopotential can regulate charge carrier separation, which is discussed below. As shown in Fig. 3b, positive and negative piezocharges were generated on the tensile and compressive strained sides of the ZnO NWs, respectively. This strain-generated piezoelectric field can facilitate the migration of photoexcited electrons and holes toward the positive and negative surfaces induced by the piezopotential, respectively, resulting in a lower recombination rate. The proposed physical and chemical reactions for the photodegradation of MB aqueous solution are shown below:

$$ZnO + h\nu \rightarrow ZnO(e_{CB}^- + h_{VB}^+)$$

$$ZnO + \text{sonication} \rightarrow ZnO(e_{\text{positive surface}}^- + h_{\text{negative surface}}^+)$$

$$ZnO(h_{VB}^+) + OH^- \rightarrow {}^{\cdot}OH + ZnO$$

$$ZnO(e_{CB}^-/e_{\text{positive surface}}^-) + O_2 \rightarrow {}^{\cdot}O_2^- + ZnO$$

$$2{}^{\cdot}O_2^- + 2H_2O \rightarrow 2{}^{\cdot}HO_2 + H_2O_2$$

$$H_2O_2 \rightarrow 2{}^{\cdot}OH$$

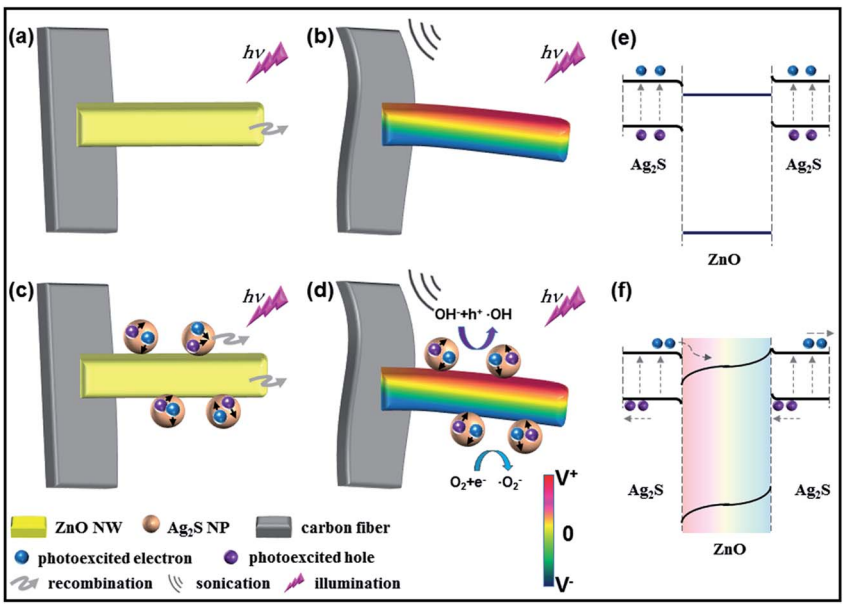

Fig. 3 Working mechanism for ZnO and Ag_2S@ZnO photocatalysts. ZnO and Ag_2S@ZnO NWs were used as photocatalysts under light irradiation (a, c) without and (b, d) with sonication, respectively. Schematic band structures of Ag_2S/ZnO NW under (e) only light illumination and (f) light illumination and sonication. To illustrate the charge separation process under sonication conditions, the background color indicates the presence of a piezopotential.

$$^{\cdot}OH + MB \rightarrow CO_2 + H_2O$$

In particular, for Ag_2S NPs on ZnO NW surfaces, electron–hole pairs can also be instantaneously photoexcited under simulated solar light illumination, as shown in Fig. 3c and e. The spatial separation of electron–hole pairs can be attributed to the type II band alignment at the Ag_2S/ZnO heterointerface. Because the CB and VB of ZnO stay below the energy band of Ag_2S, the photoexcited electrons on the Ag_2S NPs can be transported to the ZnO NWs through the heterointerface. Correspondingly, photoexcited holes can be induced to the heterointerface region. Notably, the effective separation of photoexcited electrons and holes in the Ag_2S@ZnO composite is driven by the strain-generated piezopotential, as shown in Fig. 3d and f. On one hand, photoexcited electrons from Ag_2S NPs were transferred to the ZnO NWs, which can promote the reaction to produce free hydroxyl radicals ($^{\cdot}OH$), while on the other hand, photoexcited holes from Ag_2S NPs preferred to shift to the Ag_2S/ZnO heterointerface and Ag_2S NP surface, which played an important role in photodegradation. Under sonication and light illumination conditions, MB in aqueous solution was decomposed due to the effective separation of photoexcited electron–hole pairs aided by the strain-generated piezopotential. The additional reactions involved in MB photodegradation by Ag_2S@ZnO NWs are shown below:

$$Ag_2S + h\nu \rightarrow Ag_2S(e_{CB}^- + h_{VB}^+)$$

$$Ag_2S(e_{CB}^-) + ZnO \rightarrow Ag_2S + ZnO(e_{CB}^-)$$

$$Ag_2S + ZnO(h_{VB}^+) \rightarrow Ag_2S(h_{VB}^+) + ZnO$$

$$Ag_2S(h_{VB}^+) + MB \rightarrow Ag_2S + CO_2 + H_2O$$

Fig. 3e shows the relative valence and conduction band positions of Ag_2S@ZnO composite under strain-free condition. At the Ag_2S/ZnO heterointerface, a CB offset (ΔE_c) of 0.14 eV and a VB offset (ΔE_v) of 2.05 eV were present. The staggered band alignment has been reported to facilitate photoexcited charge carriers passing through the heterointerface.[16] Therefore, spatially separated electrons and holes can be efficiently utilized in the photocatalytic activity. Notably, the separation of photoexcited charge carriers was further promoted by the strain-generated piezopotential, which effectively suppresses the recombination of electron–hole pairs. This piezopotential, induced by the positive and negative piezocharges, can encourage photoexcited electrons and holes to migrate to positive and negative piezopotential surfaces, respectively, of bent ZnO NWs. Moreover, positive piezocharges are accumulated at the heterointerface region, which can slightly reduce the barrier height to help electrons transfer from Ag_2S NPs to ZnO NWs. Therefore, a large number of photoexcited charge carriers could be utilized in the photocatalytic process before unfavorable recombination, which was a prominent characteristic of the piezopotential-enhanced hybrid photocatalyst.

The performances of ZnO and Ag_2S@ZnO NWs photocatalysts in the degradation of MB aqueous solution were investigated under light irradiation and/or sonication conditions. The adsorption–desorption equilibrium between MB and the as-prepared photocatalyst was achieved by immersing the ZnO NWs (or Ag_2S@ZnO NWs) in MB aqueous solution for 1 h. During this period, the MB aqueous solution was magnetically stirred under ambient conditions before each catalytic experiment. The initial concentration of MB aqueous solution (denoted as C_0, C_0 = 1.0 mg mL^{-1}) and final concentration (residual concentration of MB; denoted as C) were characterized by UV-Vis spectroscopy. The degradation rate (denoted as C/C_0) was calculated for different photocatalysts and experimental conditions. Absorption spectra of MB aqueous solution after applying light irradiation or sonication were recorded at time intervals of 1 h, as shown in Fig. 4. Slight differences in the performance of ZnO NWs catalysts tested under different conditions were observed after reacting for 2 h (C/C_0 = 46.1% for sonication and 49.0% for light illumination), which showed that slow degradation of the organic dye can be achieved using a photocatalytic process or a piezopotential/piezocharge-triggered catalytic process in the dark. To confirm that these two strategies are compatible for enhancing photocatalytic performance, further experiments were conducted by simultaneously applying light illumination and sonication to the MB aqueous solution. MB decomposition in aqueous solution reached 88.2% after 2 h and was complete after 4 h. Our results indicated the increased amount of effective charge carriers produced by sonication was involved in the photocatalytic process, which demonstrates that the piezotronic effect can enhance the photocatalytic reaction. We then investigated the Ag_2S@ZnO NW samples to further promote photocatalytic performance by introducing piezopotentials/piezocharges into the heterojunctions/interfaces formed by Ag_2S and ZnO. Compared to the ZnO NWs sample, Ag_2S@ZnO NWs exhibited much improved catalytic efficiency when applying individual sonication or light illumination (C/C_0 = 17.6% for light illumination and 8.8% for sonication after 2 h). Complete MB decomposition was achieved within 2 h by applying simultaneous light illumination and sonication, which represented enhanced photocatalytic performance compared with bare ZnO

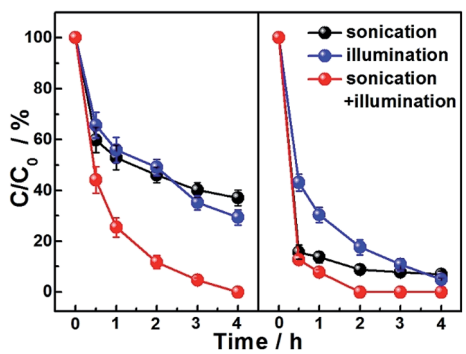

Fig. 4 MB degradation rate as a function of reaction time with ZnO (left) and Ag_2S@ZnO (right) NWs measured under simulated solar light illumination (320–800 nm) and/or sonication (~80 mW cm^{-2}).

NWs. The absorption spectra of MB aqueous solutions using ZnO and Ag_2S@ZnO NWs catalysts under different experimental conditions were compared, as shown in Fig. S3 (ESI†). Based on our experimental data and theoretical analysis, it was concluded that the strain-generated piezopotentials/piezocharges regulated the charge carrier generation and separation process. A comparison of dye degradation behavior between using only light irradiation and simultaneously applying light irradiation and sonication undoubtedly showed that the strain-generated piezopotentials/piezocharges improved the photocatalytic performances of ZnO and Ag_2S@ZnO NWs. This combined effect of photoexcited charge carriers and piezocharges indicated the contribution of the piezotronic effect to the photocatalytic activity. The combined effect became insignificant for Ag_2S@ZnO NWs due to the comparable dye degradation rates within 1 h for Ag_2S@ZnO NW when individually applying light irradiation and simultaneously applying light irradiation and sonication. After reacting for 2 h (Fig. 4), Ag_2S@ZnO had clearly achieved maximum MB degradation with the assistance of photoexcited charge carriers and piezocharges, because photoexcited charge carriers from Ag_2S NPs can be effectively employed for photocatalysis based on the piezotronic effect. Detailed studies on different concentrations of organic dye using Ag_2S@ZnO will be presented in future and help to achieve a quantitative understanding of this combined effect and further optimize the photocatalytic performance using other piezoelectric semiconductors.

Compared to ZnO NWs, Ag_2S@ZnO NWs demonstrated better reproducibility in the photocatalytic degradation. The cycling performance of Ag_2S@ZnO NWs is shown in Fig. 5. In the first six cycles, a large difference in the MB degradation rates of ZnO NWs ($C/C_0 = 28.4\%$) and Ag_2S@ZnO NWs ($C/C_0 = 6.9\%$) was found. After eight cycles, more than 80% of MB in solution was decomposed by Ag_2S@ZnO NWs within 4 h. However, for ZnO NWs without Ag_2S NPs, 48.1% of MB remained in solution after eight cycles. According to previous studies, photocorrosion is responsible for the decrease in degradation rate. As the ZnO NW surfaces were slightly protected by Ag_2S NPs, the reproducibility and stability of Ag_2S@ZnO NWs was strongly enhanced. Moreover, we performed SEM and XRD characterization of the ZnO and Ag_2S@ZnO NWs after the photocatalytic reaction. Both ZnO and Ag_2S@ZnO NWs had maintained their 1D morphologies, as shown in Fig. S4 (ESI†). However, the surface of bare ZnO NWs had become rough due to photocorrosion, while no significant morphology change was observed in Ag_2S@ZnO NWs. Furthermore, SEM data showed that ZnO and Ag_2S@ZnO nanowires survived under sonication condition for several cycles (see Fig. S5 in ESI†). XRD spectra of ZnO and Ag_2S@ZnO NWs were recorded after eight photocatalytic cycles, and showed characteristic signals for their ZnO and Ag_2S components, as shown in Fig. S6 (ESI†). In contrast to photocatalysts with nanoparticle morphology previously reported, Ag_2S@ZnO NWs were synthesized and fixed on a flexible carbon fiber that could be easily recovered in a labor-saving process to avoid photocatalyst loss.[41,52] Our results indicated that efficient photocatalysts can be synthesized from inexpensive and environmentally friendly inorganic composites with

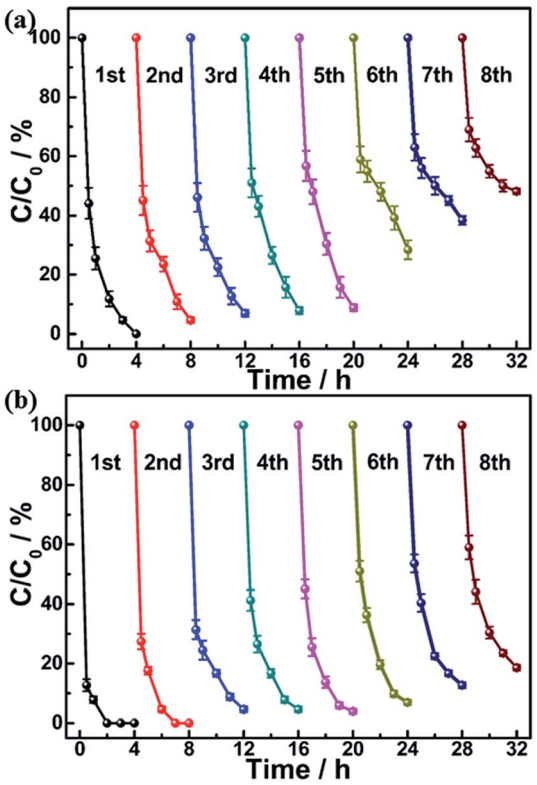

Fig. 5 Cyclic MB degradation curves as a function of reaction time for (a) ZnO and (b) Ag_2S@ZnO NWs, measured under simulated solar light and sonication condition.

contribution from piezoelectric semiconductors. We have summarized relevant reports on ZnO-based photocatalysts, including doped ZnO and nanocomposites in Table S1 (ESI†). A comparison of their photocatalytic performances demonstrated that both chemical doping and surface modification effectively improved the photocatalytic activity. Moreover, Ag_2S@ZnO NWs demonstrated enhanced photocatalytic performance due to the additional contribution of the piezotronic effect.

Conclusions

In summary, we have demonstrated a promising strategy for enhancing the photocatalytic performance of Ag_2S@ZnO composites on common carbon fiber cloth using strain-induced piezopotentials/piezocharges. The environmentally friendly, low-cost, and scalable synthesis of Ag_2S@ZnO NWs was performed using a combination of hydrothermal and SILAR methods. The non-piezoelectric Ag_2S and piezoelectric ZnO components exhibited respective contributions to improving visible light absorption and promoting photoexcited charge carrier separation. Our results demonstrated a large improvement in photocatalytic and recycling performance for MB degradation in aqueous solution under simultaneous light illumination and sonication conditions owing to the piezotronic effect. The enhanced photocatalytic performance of Ag_2S@ZnO NWs compared with ZnO NWs was attributed to strain-generated piezopotentials/piezocharges from the bent

ZnO NWs, which facilitated electron and holes transport across the Ag_2S/ZnO heterointerface with a staggered type II band alignment. For practical application to water purification, our results provide useful information regarding not only ZnO-based nanomaterials, but also other piezoelectric semiconductors with smaller band gaps.

Conflicts of interest

There are no conflicts of interest to declare.

Acknowledgements

This work was supported by the National Natural Science Foundation of China (Grant No. 51472056, 51502017 and 21603014), the "Thousands Talents" program for pioneer researchers and their innovation team, China, and the Recruitment Program of Global Youth Experts, China.

References

1 M. M. Pendergast and E. M. V. Hoek, *Energy Environ. Sci.*, 2011, **4**, 1946.
2 A. G. Fane, R. Wang and M. X. Hu, *Angew. Chem., Int. Ed.*, 2015, **54**, 3368.
3 R. Asahi, T. Morikawa, H. Irie and T. Ohwaki, *Chem. Rev.*, 2014, **114**, 9824.
4 A. Kubacka, M. Fernandez-Garcia and G. Colon, *Chem. Rev.*, 2012, **112**, 1555.
5 M. D. Hernandez-Alonso, F. Fresno, S. Suarez and J. M. Coronado, *Energy Environ. Sci.*, 2009, **2**, 1231.
6 D. Ravelli, D. Dondi, M. Fagnoni and A. Albini, *Chem. Soc. Rev.*, 2009, **38**, 1999.
7 V. Devabhaktuni, M. Alam, S. S. S. R. Depuru, R. C. Green, D. Nims and C. Near, *Renewable Sustainable Energy Rev.*, 2013, **19**, 555.
8 R. Marschall, *Adv. Funct. Mater.*, 2014, **24**, 2421.
9 Y. C. Lan, Y. L. Lu and Z. F. Ren, *Nano Energy*, 2013, **2**, 1031.
10 J. Tian, Z. Zhao, A. Kumar, R. I. Boughton and H. Liu, *Chem. Soc. Rev.*, 2014, **43**, 6920.
11 M. Y. Wang, J. Ioccozia, L. Sun, C. J. Lin and Z. Q. Lin, *Energy Environ. Sci.*, 2014, **7**, 2182.
12 Y. Tak, H. Kim, D. Lee and K. Yong, *Chem. Commun.*, 2008, 4585.
13 C. An, J. Liu, S. Wang, J. Zhang, Z. Wang, R. Long and Y. Sun, *Nano Energy*, 2014, **9**, 204.
14 D. T. Yue, X. F. Qian and Y. X. Zhao, *Sci. Bull.*, 2015, **60**, 1791.
15 S. S. Lo, T. Mirkovic, C. H. Chuang, C. Burda and G. D. Scholes, *Adv. Mater.*, 2011, **23**, 180.
16 D. Hong, W. Zang, X. Guo, Y. Fu, H. He, J. Sun, L. Xing, B. Liu and X. Xue, *ACS Appl. Mater. Interfaces*, 2016, **8**, 21302.
17 L. Wang, J. Ge, A. Wang, M. Deng, X. Wang, S. Bai, R. Li, J. Jiang, Q. Zhang, Y. Luo and Y. Xiong, *Angew. Chem., Int. Ed.*, 2014, **53**, 5107.
18 M. Y. Xing, B. X. Yang, H. Yu, B. Z. Tian, S. Bagwasi, J. L. Zhang and X. Q. Gongs, *J. Phys. Chem. Lett.*, 2013, **4**, 3910.
19 Z. Y. Zhang, Z. Wang, S. W. Cao and C. Xue, *J. Phys. Chem. C*, 2013, **117**, 25939.
20 X. Yu, A. Shavel, X. An, Z. Luo, M. Ibanez and A. Cabot, *J. Am. Chem. Soc.*, 2014, **136**, 9236.
21 K. Dong, L. Huang, C. Wang, P. Xu, Y. Zhang, C. Feng, T. Chen, Q. Wang and Y. Zhang, *RSC Adv.*, 2017, **7**, 16535.
22 N. Riaz, F. K. Chong, Z. B. Man, M. S. Khan and B. K. Dutta, *Ind. Eng. Chem. Res.*, 2013, **52**, 4491.
23 L. F. Chiang and R. A. Doong, *J. Hazard. Mater.*, 2014, **277**, 84.
24 Y. J. Yao, C. Xu, J. C. Qin, F. Y. Wei, M. N. Rao and S. B. Wang, *Ind. Eng. Chem. Res.*, 2013, **52**, 17341.
25 J. M. Liu, L. Han, H. Y. Ma, H. Tian, J. C. Yang, Q. C. Zhang, B. J. Seligmann, S. B. Wang and J. Liu, *Sci. Bull.*, 2016, **61**, 1543.
26 W. Wu and Z. L. Wang, *Nat. Rev. Mater.*, 2016, **1**, 16031.
27 Z. L. Wang, *Adv. Mater.*, 2007, **19**, 889.
28 Z. L. Wang, *Adv. Mater.*, 2012, **24**, 4632.
29 C. Liu, M. Peng, A. Yu, J. Liu, M. Song, Y. Zhang and J. Zhai, *Nano Energy*, 2016, **26**, 417.
30 D. Y. Kim, S. Lee, Z. H. Lin, K. H. Choi, S. G. Doo, H. Chang, J. Y. Leem, Z. L. Wang and S. O. Kim, *Nano Energy*, 2014, **9**, 101.
31 M. Song, Y. Zhang, M. Z. Peng and J. Y. Zhai, *Nano Energy*, 2014, **6**, 66.
32 Y. Zhang, C. Liu, J. Liu, J. Xiong, J. Liu, K. Zhang, Y. Liu, M. Peng, A. Yu, A. Zhang, Y. Zhang, Z. Wang, J. Zhai and Z. L. Wang, *ACS Appl. Mater. Interfaces*, 2016, **8**, 1381.
33 C. Liu, A. Yu, M. Peng, M. Song, W. Liu, Y. Zhang and J. Zhai, *J. Phys. Chem. C*, 2016, **120**, 6971.
34 X. Y. Xue, W. L. Zang, P. Deng, Q. Wang, L. L. Xing, Y. Zhang and Z. L. Wang, *Nano Energy*, 2015, **13**, 414.
35 X. Guo, Y. Fu, D. Hong, B. Yu, H. He, Q. Wang, L. Xing and X. Xue, *Nanotechnology*, 2016, **27**, 375704.
36 J. Yu and X. Yu, *Environ. Sci. Technol.*, 2008, **42**, 4902.
37 T. Xia, P. Wallenmeyer, A. Anderson, J. Murowchick, L. Liu and X. B. Chen, *RSC Adv.*, 2014, **4**, 41654.
38 F. Xu, J. Chen, L. Y. Guo, S. Y. Lei and Y. R. Ni, *Appl. Surf. Sci.*, 2012, **258**, 8160.
39 N. T. Khoa, S. W. Kim, D. V. Thuan, D. H. Yoo, E. J. Kim and S. H. Hahn, *CrystEngComm*, 2014, **16**, 1344–1350.
40 J. S. Hu, L. L. Ren, Y. G. Guo, H. P. Liang, A. M. Cao, L. J. Wan and C. L. Bai, *Angew. Chem., Int. Ed.*, 2005, **44**, 1269.
41 H. D. Li, Y. H. Sang, S. J. Chang, X. Huang, Y. Zhang, R. S. Yang, H. D. Jiang, H. Liu and Z. L. Wang, *Nano Lett.*, 2015, **15**, 2372.
42 J. Xu, Z. Chen, J. A. Zapien, C. S. Lee and W. Zhang, *Adv. Mater.*, 2014, **26**, 5337.
43 M. Gholami, M. Qorbani, O. Moradlou, N. Naseri and A. Z. Moshfegh, *RSC Adv.*, 2014, **4**, 7838.
44 Y. Zhang, B. K. Liu, D. J. Wang, Y. H. Lin, T. F. Xie and J. L. Zhai, *Mater. Chem. Phys.*, 2012, **133**, 834.
45 S. Khanchandani, P. K. Srivastava, S. Kumar, S. Ghosh and A. K. Ganguli, *Inorg. Chem.*, 2014, **53**, 8902.
46 C. Chen, Z. Li, H. Lin, G. Wang, J. Liao, M. Li, S. Lv and W. Li, *Dalton Trans.*, 2016, **45**, 3750.

47 I. G. Theodorou, Z. A. Jawad, H. Qin, E. O. Aboagye, A. E. Porter, M. P. Ryan and F. Xie, *Nanoscale*, 2016, **8**, 12869.
48 T. Hirakawa and P. V. Kamat, *J. Am. Chem. Soc.*, 2005, **127**, 3928.
49 G. Williams, B. Seger and P. V. Kamat, *ACS Nano*, 2008, **2**, 1487.
50 V. Subramanian, E. Wolf and P. V. Kamat, *J. Phys. Chem. B*, 2001, **105**, 11439.
51 J. Mu, C. Shao, Z. Guo, Z. Zhang, M. Zhang, P. Zhang, B. Chen and Y. Liu, *ACS Appl. Mater. Interfaces*, 2011, **3**, 590.
52 L. Wang, S. Liu, Z. Wang, Y. Zhou, Y. Qin and Z. L. Wang, *ACS Nano*, 2016, **10**, 2636–2643.